*Published online 31 August 2012* *Nucleic Acids Research, 2012, Vol. 40, No. 20* ***10543–10553***
*doi:10.1093/nar/gks791*

# Metal and ligand binding to the HIV-RNase H active site are remotely monitored by Ile556

**Xunhai Zheng, Geoffrey A. Mueller, Eugene F. DeRose and Robert E. London***

Laboratory of Structural Biology, NIEHS, National Institutes of Health, Research Triangle Park, NC 27709, USA

Received April 25, 2012; Revised July 26, 2012; Accepted July 27, 2012

## ABSTRACT

**HIV-1 reverse transcriptase (RT) contains a C-terminal ribonuclease H (RH) domain on its p66 subunit that can be expressed as a stable, although inactive protein. Recent studies of several RH enzymes demonstrate that substrate binding plays a major role in the creation of the active site. In the absence of substrate, the C-terminal helix E of the RT RNase H domain is dynamic, characterized by severe exchange broadening of its backbone amide resonances, so that the solution characterization of this region of the protein has been limited. Nuclear magnetic resonance studies of $^{13}$C-labeled RH as a function of experimental conditions reveal that the $\delta$1 methyl resonance of Ile556, located in a short, random coil segment following helix E, experiences a large $^{13}$C shift corresponding to a conformational change of Ile556 that results from packing of helix E against the central β-sheet. This shift provides a useful basis for monitoring the effects of various ligands on active site formation. Additionally, we report that the RNase H complexes formed with one or both divalent ions can be individually observed and characterized using diamagnetic $Zn^{2+}$ as a substitute for $Mg^{2+}$. Ordering of helix E results specifically from the interaction with the lower affinity binding to the A divalent ion site.**

## INTRODUCTION

HIV-1 reverse transcriptase (RT) converts single-stranded viral RNA into double-stranded DNA for subsequent incorporation into the host cell genome. The RT p66 subunit contains a C-terminal ribonuclease H (RH) domain that is responsible for degrading the RNA template of the hybrid RNA•DNA form of the viral genome (1). Concepts of the catalytic mechanism and active site structure of RNase H enzymes have evolved significantly in recent years as a result of the availability of structural data for RNase H complexes with the RNA•DNA substrate (2–4). These results, combined with theoretical analyses (5,6), provide compelling support for a catalytic model involving two divalent cations that function to activate the nucleophile and to stabilize the transition state (4). As a result of the emergence of drug-resistant mutated forms of RT, the targeting of additional sites such as the RNase H domain of RT has attracted considerable attention (7–10).

Kinetic, mutational and structural studies have established the functional importance of residues located in the C-terminus of the RNase H domain (2,11–13). Residue Asp549 on C-terminal helix E (residues 543–554) is one of the four acidic residues of the DEDD motif that bind the two catalytically important divalent metal ions (2). Deletion of the 16 C-terminal residues (545–560) has been reported to eliminate RH activity (11). There is also evidence for a functional role of the C-terminal residues that follow helix E; deletion of the eight C-terminal residues on the p66 subunit of RT (553–560) does not eliminate RH activity, but leads to a loss of strand transfer activity (11). Mutations of Lys558 are statistically associated with a number of thymidine analog resistance mutations (TAMs), suggesting that these mutations reinforce nucleoside drug resistance (13). In addition to its importance as a drug target, the RNase H domain of RT has been studied as a model for protein folding (14,15).

Despite the functional importance of divalent ions and the C-terminal residues of the RNase H domain, nuclear magnetic resonance (NMR) studies indicate that, even in the presence of physiological levels of $Mg^{2+}$ ions, these residues are dynamic and not well ordered (15–18). For the isolated RH domain the backbone amide resonances of the C-terminal helix E exhibit significant exchange broadening so that the region between residues 545 and 554 is difficult to observe (15,16,18). In contrast, amide resonances from 555 to 560 are fairly intense and their shifts are indicative of a random coil structure. The exchange broadening of the helix E resonances suggests that there is some pre-assembly of the active site helix

*To whom correspondence should be addressed. Tel: +1 919 541 4879; Fax: +1 919 541 5707; Email: london@niehs.nih.gov

since, unlike the resonances of the six C-terminal residues, they do not exhibit random coil characteristics. Similarly, crystallographic studies of apo RT structures sometimes do not reveal helix E and rarely reveal any of the post-helical residues, also consistent with a dynamic structure. Thus, the structure of the RNase H active site in the presence of its substrate differs substantially from that of the apo enzyme, which is incompletely formed and considerably more dynamic. This behavior contrasts with many enzymes that utilize a well-formed active site to achieve high substrate selectivity and catalytic efficiency. A complete understanding of the catalytic behavior and, from a practical standpoint, the development of RNase H inhibitors requires an understanding of the transformation of the RNase H active site from the dynamic, partially disordered, incompletely coordinated state of the apo enzyme to the ordered state characterizing the substrate complex. In view of the limited insight available from analysis of the backbone resonances, we have examined the behavior of resonances of the amino acid sidechains. There has been substantial recent progress in utilizing sidechain resonance shifts for conformational analysis (19–22). Remarkably, we demonstrate that the δ1 methyl resonance arising from Ile556, located in the post-helical random coil segment of the sequence, provides significant insights into the behavior of helix E and the assembly of the active site. Furthermore, this resonance can serve as a useful indicator for investigating the dependence of active site formation on divalent metal ions and other experimental conditions, and for the identification of other ligands that influence RNase H active site stability.

## MATERIALS AND METHODS

The constructs used were identical to those used in previous studies and the labeled RNase H domain was produced following a protocol modified from that described previously (18,23). Briefly, the collected cell pellets were suspended in 50 mM Tris–HCl, 5% Glycerol pH 8.0 and lysed by sonication. The lysate was centrifuged at 30 000*g* for 30 min. The lysate supernatant was loaded onto a HiTrap SP HP column in tandem with a HiTrap QP HP column, and washed with 50 mM Tris–HCl pH 8.0 until the $OD_{280}$ value of flow through approached zero. The QP HP column was gradient eluted with 1 M NaCl in 50 mM Tris–HCl, 5% Glycerol pH 8.0. The RNase H-containing fractions were pooled based on SDS–PAGE results. The pooled RNase H was concentrated to a small volume and loaded on the pre-equilibrated HiLoad 26/60 Superdex-200 column with 50 mM Tris–HCl, 200 mM NaCl 1 mM EDTA pH 8.0 buffer. All of the above procedures were carried out at 4°C. The RNase H domain mutants, H539S and R557S, were produced using the Quickchange mutagenesis kit (Stratagene, Inc., La Jolla, CA, USA). Expression and purification of the mutants was identical to procedures used for the wild-type enzyme. Subunit-specific labeling of HIV-1 RT was implemented as described previously (23) except that in the present case, we utilized a [4-$^{13}$C,3,3-$^{2}H_2$]2-oxobutyrate labeling precursor in a deuterated growth medium (24).

The RNase H sequence used in this and our previous studies (18,25) corresponds to the HXB2 sequence contained in the HIV sequence compendium (26)with an additional N-terminal MNEL leader sequence that precedes Tyr427. In the present study, we have followed the standard numbering of the RNase H domain in the p66 subunit, while in our earlier BMRB entries, the residues were numbered from the N-terminus of the isolated construct. The residue identifications in the BMRB entries can be converted into the standard numbering by adding 422. The exact sequence is included as Supplementary Figure S1. Assignments of the isoleucine δ-$^{13}CH_3$ resonances were based on a comparison of the $^{1}$H–$^{13}$C HMQC spectrum of [δ-$^{13}CH_3$-Ile]RNase H obtained in 80 mM $Mg^{2+}$ with the previous entries determined under similar conditions (BMRB 5347), subject to two changes: first, the specific isoleucine Cδ-labeled sample indicates that the previous assignments of the Ile521 Cδ and Cγ2 resonances need to be reversed. Second, the unusual shift and exchange broadening of Ile556 Cδ resonance apparently resulted in an incorrect assignment of this resonance in BMRB 5347. The correct assignment can be made by exclusion, since each of the other nine Ile Cδ resonances is assigned using the above procedure.

The Ile434 and Ile556 δ–methyl resonances in the p66 subunit of HIV-1 RT were assigned based on their positions in the isolated RNase H domain and their relative isolation, which greatly limits the possibility of misassignment. Analogous domain-based assignment strategies have been used in similar studies of very large proteins (27,28). A more extensive study of isoleucine-labeled RT is currently in preparation.

Synthesis of the RNase H inhibitor 2-hydroxyisoquinoline-1,3(2H,4H)-dione is described by Billamboz *et al*. (29), and was obtained as a custom synthesis product from MRIGlobal (Kansas City, MO).

$^{1}$H–$^{13}$C HMQC spectra were obtained at 25°C by using Varian's gChmqc sequence on a UNITY INOVA 500 MHz spectrometer with 128 × 1024 complex points and acquisition time of 128 ms in both $t_1$ and $t_2$. Sixteen scans were acquired per increment, with a 1.0 s delay between scans. The $^{1}$H–$^{15}$N HSQC spectra of the arginine NHε region were acquired at 25°C using the Varian gNhsqc sequence. The $^{15}$N offset was set at 90 ppm. All NMR data were processed by NMRpipe (30) and analyzed with NMRViewJ program (31). Titration studies were performed on 15 μM RNase H domain in 20 mM Tris–d11. Structures were analyzed and visualized with PyMol (www.pymol.org).

The pH and Mg-induced Ile556 titration data was fit using a single $K_D$ according to the relations:

$$\delta^{13}C = c1+(c2-c1)\frac{10^{pK-pH}}{1+10^{pK-pH}} \quad (1)$$

$$\delta^{13}C = c1+(c2-c1) \times \frac{([Mg]+[RH]+K_D)-\sqrt{([Mg]+[RH]+K_D)^2-4[Mg][RH]}}{2[RH]} \quad (2)$$

where $c1$ and $c2$ are the limiting Ile shifts for the apo enzyme under high or low pH conditions, or low and high $Mg^{2+}$, respectively, and the p$K$ and $K_D$ values are also allowed to vary. For the $Mg^{2+}$ titration, the data were insufficient to allow fitting to a more complex binding model.

The $p_{HelixE}$ values calculated from the Ile556 Cδ methyl shift using the relation in the text, were subsequently fitted to Equation (1); however in this case, the $c1$ and $c2$ parameters correspond to limiting helix probabilities. Similarly, the $p_{HelixE}$ values determined as a function of $Mg^{2+}$ from the measured Ile556 Cδ methyl shift values and the relation in the text were subsequently fit to the relation:

$$p_{HelixE} = c1 + (c2 - c1)\frac{[Mg^{2+}]}{[Mg^{2+}] + K_D} \quad (3)$$

in order to evaluate the limiting behavior of $p_{HelixE}$ as a function of $Mg^{2+}$.

## RESULTS

The limited information available from analysis of the backbone resonances of the RT RNase H domain, particularly in the region of the C-terminus, led us to investigate the behavior of the sidechain resonances. Surprisingly, the spectrum of the [$^{13}$CδH$_3$-Ile] RNase H domain revealed a significant sensitivity of the Ile556 methyl resonance to pH (Figure 1 and Supplementary Figure S2). A fit of the titration data for Ile556 yields total titration shifts of $\Delta^{13}C = -2.34$ ppm; $\Delta^{1}H = -0.146$ ppm, both corresponding to a p$K = 5.77$, with the resonances moving upfield as the pH is reduced. There are no titratable residues in the sequence surrounding Ile556: LVSAGI$^{556}$RKVL$^{560}$ consistent with the observed p$K$ value, and the influence of residues more distant in sequence but in spatial propinquity is inconsistent with the disordered conformation of this segment.

There is increasing evidence that the $^{13}$C shift values for many amino acid sidechain resonances appear to be dominated by conformationally-dependent 'γ-effects' first characterized in studies of aliphatic hydrocarbons by Grant and coworkers (32,33). According to this analysis, the upfield shift observed for Ile556 δ1 methyl is typical of Ile residues with $\chi2$ in the g− conformation (19). Using the relation developed by Hansen *et al.* (21), the Ile556 $\chi2$ distribution changes from ∼45% g− conformer at neutral pH, to ∼84% g− conformer at low pH, so that its pH dependence may be qualitatively described by the relation:

$$\mathrm{Ile556}_{\chi^2=rc} \underset{\mathrm{pH}\uparrow}{\overset{\mathrm{pH}\downarrow}{\rightleftharpoons}} \mathrm{Ile556}_{\chi^2=g-}$$

where *rc* represents a random coil mixture. Since the *g*− conformation represents a less energetically favorable rotamer than the predominant *t* conformation, the high *g*− probability that characterizes the low pH behavior of Ile556 is inconsistent with a random coil state. Thus, this behavior indicates that at low pH, Ile556 experiences significant inter-residue stabilizing interactions that compensate for the higher intrinsic energy of the *g*− rotamer.

Crystallographic studies of RT provide limited information on the behavior of the RNase H C-terminus; however, recent studies of RNase H–inhibitor complexes show the positions of both bound $Mg^{2+}$ ions as well as most of the C-terminal residues (34–37). Interestingly, although none of the structures of apo RT show an Ile556 residue with a $\chi2 = g-$ conformation, all of the RNase H–inhibitor complexes show this conformation to be present (Figure 2). In each of these structures, the sidechain of Ile556 packs against the central β-sheet and continues the amphiphilic motif of Val548 and Val552. These structures reveal the role of the bound $Mg^{2+}$ ions, and particularly $Mg_A$, in stabilizing the orientation of helix E by bridging Asp443, located on the central β-sheet, and Asp549, located on helix E (Figure 2a). It is reasonable to hypothesize that the observed pH dependence of the Ile556 shift results from formation of a hydrogen bonding interaction between the same two aspartyl residues, such that the repulsive interaction at higher pH is replaced by a positive interaction as the hydrogen bond forms at lower pH. The p$K$ value of 5.77 obtained from the Ile556 shifts is well above that expected for an isolated aspartyl sidechain (38), but is consistent with a shared hydrogen bond.

We also considered the alternative hypothesis that the pH-dependent shifts of Ile556 and Ile542 might result from a conformational transition induced by titration of His539. This hypothesis is based on the proximity of His539 to Glu546 and Asp549 in some of the structures of RNaseH–inhibitor complexes, as well as the similarity of the p$K$ values obtained above to typical histidine p$K$ values. In order to evaluate the role of such interactions, we analyzed the pH behavior of the isoleucine residues in an RNase H (H539S) mutant. The titration behavior of Ile556 in the mutant is essentially unaffected by this mutation, while there is a somewhat larger perturbation of the Ile542 titration, consistent with its proximity to the mutated residue (Supplementary Figure S3). Thus, titration of His539 has no effect on the behavior of Ile556, consistent with the above interpretation that the pH-dependent effect on Helix E results from an effect on the electrostatic repulsion of the active site aspartyl residues.

It is likely that both the integrity of the helix, as well as its position is also destabilized by loss of the interactions with the β-sheet. However, the exchange broadening of the amide resonances as well as the Ile556 $^{13}$Cδ shift behavior discussed above indicate that the structure does not unwind and produce a random coil, but equilibrates between the packed conformation observed in the inhibitor complex and a partially disordered conformation. In summary, comparison of the titration data with the structures of RNase H–inhibitor complexes strongly suggests that lowering the sample pH is exerting a conformational effect that is in some respects analogous to the conformation observed for the $Mg^{2+}$–inhibitor complexes.

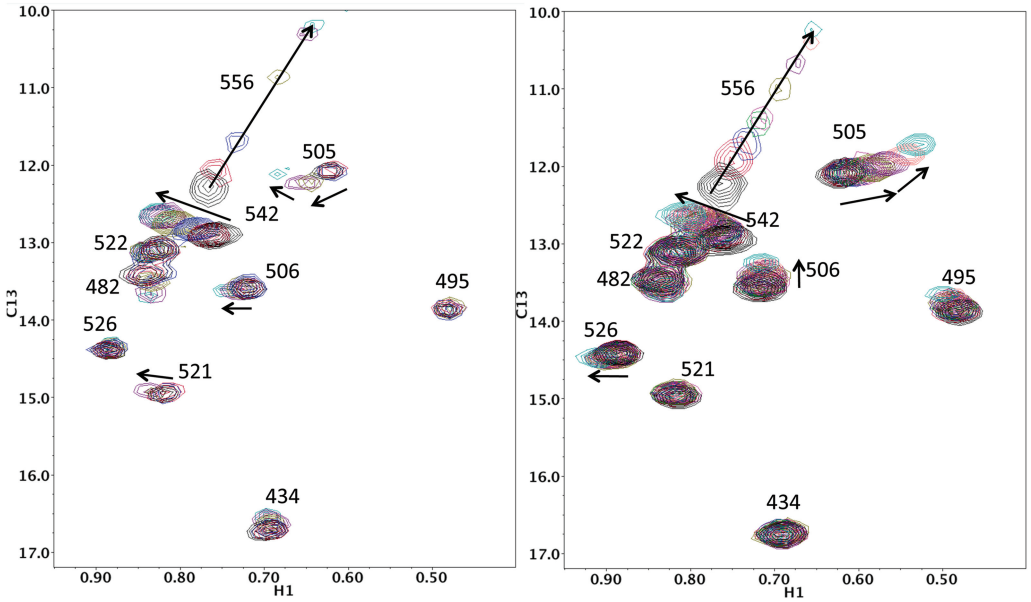


**Figure 1.** pH and $Mg^{2+}$ titration of the Cδ resonances of [$^{13}$CδH$_3$-Ile]RNase H domain from HIV-1 RT. The construct is identical to that used in previous studies (18), and labeling was achieved by growth on a medium containing [4-$^{13}$C,3,3,-$^{2}$H$_2$]2-oxobutyrate. (**a**) pH titration; color coding for pH 7.1, 6.6, 6.1, 5.5, 5.0, 4.5 is black, red, blue, gold, purple, and cyan, respectively. (**b**) Magnesium titration of RNase H at pH 7.1; color coding for [$Mg^{2+}$] = 0, 1, 2, 3, 4, 8, 16, 32, 64 mM is black, red, blue, green, magenta gold, purple, orange, cyan. $^{1}$H–$^{13}$C HMQC spectra were obtained at 25°C by using Varian's gChmqc sequence on a UNITY INOVA 500 MHz spectrometer with 128 × 1024 complex points and acquisition time of 128 ms in both $t_1$ and $t_2$. Sixteen scans were acquired per increment, with a 1.0 s delay between scans. Titration studies used 15 μM RNase H domain in 20 mM Tris–dll in 100%$D_2O$.

## Effects of divalent metal ions

Based on the above analysis, we also titrated the RNase H sample with $MgCl_2$. The binding of $Mg^{2+}$ influences the Ile556 Cδ shift similarly to a pH reduction (Figure 1b). Interestingly, the Ile556 and (smaller) Ile542 shift responses to both $H^+$ and $Mg^{2+}$ are qualitatively similar, while the responses of the remaining methyl groups are very different (Figure 1a and b). This result is consistent with the conclusion that Ile542 and Ile556 are sensitive to the changing position/stability of helix E, while for the remaining isoleucine resonances, $H^+$ and $Mg^{2+}$ exert different conformational effects. Analysis of the $Mg^{2+}$ titration study yielded an apparent $K_D^{Mg}$ of 6.3 mM (Supplementary Figure S4), falling between the values of 3.2 and ~35 mM previously obtained for $Mg^{2+}$ binding to the apo RNase H domain (18). This intermediate apparent $K_D^{Mg}$ value probably results from partial occupancy of both the A and B divalent ion sites, since A-site binding would be expected to have a much more significant stabilizing effect on helix E.

Crystal structures of the isolated HIV-1 RT RNase H domain (39) and the *Escherichia coli* RNase HI (40) in the presence of $Mn^{2+}$ indicate that both divalent ion positions are occupied. In order to achieve an analogous occupation of both divalent ion sites without the associated paramagnetic effects on resonance linewidth, we utilized another transition metal ion, $Zn^{2+}$. The ionic radii of $Zn^{2+}$ and $Mg^{2+}$ are nearly identical, and it has been reported that optimal RT Rnase H activity is achieved at ~25 μM $Zn^{2+}$, much lower than the concentration of $Mg^{2+}$ required for optimal activity (although the maximum rate obtained with $Zn^{2+}$ is substantially below that determined in the presence of $Mg^{2+}$) (41). Addition of $Zn^{2+}$ at a 1:1 molar ratio with RNase H results in small shift changes for several isoleucine methyl resonances, particularly Ile482 and Ile505 but produces a minimal perturbation of the Ile556 resonance (Figure 3). This result is consistent with the conclusion that the initially bound $Zn^{2+}$ ion exhibits sufficient differential affinity for the A and B sites such that only the higher affinity B site is significantly occupied, and selective occupation of site B by a divalent ion is insufficient to significantly influence the stability of helix E (Figure 2a). Further addition of $Zn^{2+}$ to produce a 2:1 complex results in a large, upfield shift of Ile556, with the $\delta^{13}C = 9.8$ ppm (Figure 3b), lower than the values observed at low pH or at 64 mM $Mg^{2+}$ (~10.3 ppm). These results clearly indicate that at a 2:1 ratio, both divalent ion sites are largely occupied, with the occupation of site A resulting in significant helix E stabilization. The more readily resolved Ile505 resonance also shows clearly the effects of the two separate $Zn^{2+}$ complexes that are formed. Formation of the 1:1 complex produces a shift to a slightly lower $\delta^{13}C \sim 11.9$ ppm value. Subsequent formation of the 2:1 complex results in a distinct resonance with a larger $\delta^{13}C \sim 12.4$ ppm (Figure 3b). Further increases in the $Zn^{2+}$ concentration resulted in only very small additional shifts of the Ile556 resonance, although the resonance becomes more intense, consistent with a reduction in the exchange broadening (Supplementary Figure S5).

The $^{1}$H–$^{13}$C HMQC spectrum of the [$^{13}$CδH$_3$-Ile]RNase H–$Mn^{2+}$ complex was also obtained; however, the paramagnetic broadening produced by the $Mn^{2+}$ ion prevents

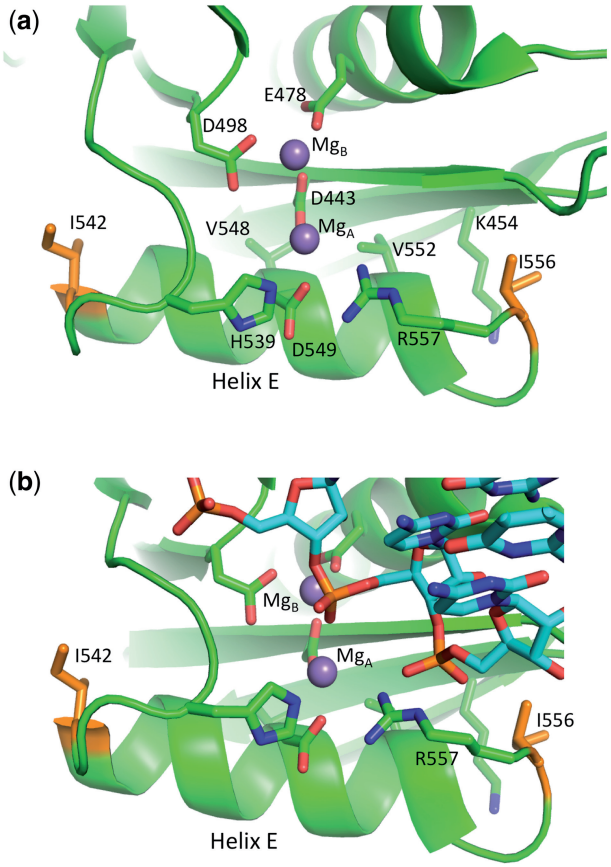


**Figure 2.** Crystal structure of the active site of the HIV RT RNase H domain. (**a**) Isolated RT RNase H domain–inhibitor complex [pdb code: 3K2P (34)].The inhibitor, which binds to both Mg ions, is not shown. The four acidic residues that complex the two Mg ions are shown, along with residues Val548, Val552 and Ile556 that mediate the interaction of helix E with the central β-sheet. Residue Ile556, indicated in orange, adopts a g− conformation for $\chi 2$. (**b**) Active site region of RT RNse H domain with bound RNA•DNA hybrid modeled into the active site. The model is based on an overlay with the structure of the human RNase HI RNA•DNA complex [pdb code 2QKK(3)].

observation of the isoleucine methyl resonances arising from the closer Ile482, Ile542 and Ile556 residues (Supplementary Figure S6).

### Effect of a $Mg^{2+}$–inhibitor complex and evaluation of a helix probability factor

As is apparent from Figure 1b, even at 64 mM $Mg^{2+}$, the Ile556 resonance exhibits substantial exchange broadening, indicating that even very high $Mg^{2+}$ concentrations are insufficient to strongly stabilize the completely folded state of the RNase H domain. Similarly, the backbone amide resonances of helix E remain difficult to observe even in the presence of high $Mg^{2+}$ (18). In order to evaluate the behavior of a more completely stabilized ternary complex, we obtained a representative dual $Mg^{2+}$-binding ligand, 2-hydroxyisoquinoline-1,3(2H,4H)-dione, the synthesis of which has been described by Billamboz *et al.* (29).

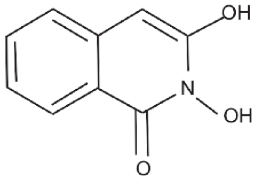


The 2-hydroxyisoquinolone and structurally related ligands interact with both $Mg_A$ and $Mg_B$, forming a stable RNaseH•$Mg^{2+}$•isoquinolone complex. Addition of 4 mM $Mg^{2+}$ + 0.5 mM isoquinolone ligand resulted in further spectral changes, such that the Ile556 $^{13}C\delta$ is shifted to a more extreme position ($\delta^{13}C = 8.6$ ppm), and the exchange broadening is dramatically reduced (Figure 4a). Thus, we assign this Ile556 shift to Ile556 locked in the $\chi 2$ = g− conformation characteristic of the fully folded state (21).

Since Ile556 is not located directly in the active site, the shift behavior of the Ile556 Cδ resonance can be used to provide an estimate for the formation of helix E as a function of different experimental conditions that is largely independent of the details of active site structure and ligands. Defining the probability of a well-formed helix to be 1 in the presence of both $Mg^{2+}$ and the isoquinolone inhibitor, and estimating that in the absence of a helix, the shift parameters for this Ile556 should be similar to those of a random coil (42), we obtain:

$$p_{HelixE} = \frac{\delta^{13}_{rc} - \delta^{13}_{obs}}{\delta^{13}_{rc} - \delta^{13}_{Mg-Inh}} = \frac{12.9 - \delta^{13}_{obs}}{12.9 - 8.6} = \frac{12.9 - \delta^{13}_{obs}}{4.3} \qquad (4)$$

Using this expression, the helix E orientational probability varies from ~14% at pH 7.1 up to ~63% at pH 4.5 (Figure 5). These values are generally consistent with the observed exchange broadening that makes the backbone amide resonances difficult to observe. Even a pH of 4.5 or a $Mg^{2+}$ concentration of 64 mM is insufficient to stabilize the helix by >~65%. We note that the calculation of Equation (4) provides an estimate of the helix E orientational probability in RNase H based on the behavior of the Ile556 resonance, and is distinct from the *g*− estimate that can be made using the relation given by Hansen *et al.* (21), which is based on an analysis of the relationship between $\delta(C^{\delta 1})$ and $^3J(C^{\delta 1},C^{\alpha})$values for the residues in a set of six proteins.

### Behavior of the RNase H domain in full RT

In order to evaluate whether a similar transition can be observed for the full RT molecule, we prepared [$^{13}C\delta H_3$-Ile]$_{66}$RT, containing isoleucine Cδ methyl labels in the p66 subunit. In the spectrum of RT obtained in the absence of $Mg^{2+}$, the resonance for Ile556 was not readily apparent, possibly due to overlap with other resonances or to more severe exchange broadening. Surprisingly, addition of 4 mM $Mg^{2+}$ was found to produce a much more extreme shift for Ile556 in RT than in the isolated RNase H domain (9.7 versus 11.4 ppm) (Figure 4b). In the full RT molecule, the N-terminus of helix E including Ile542

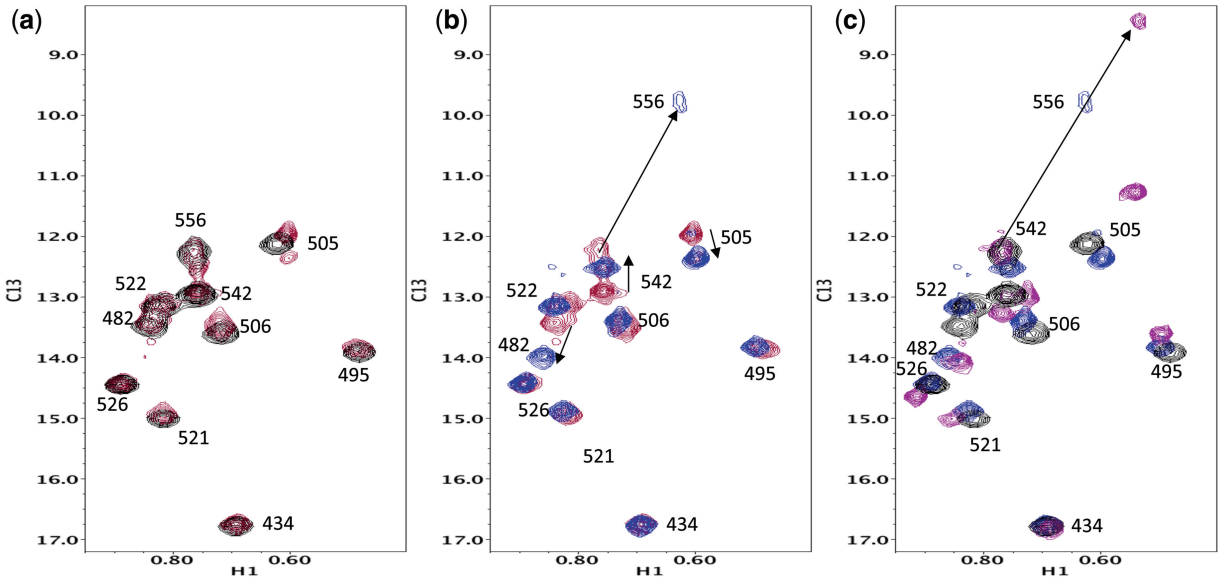


**Figure 3.** Effect of $Zn^{2+}$ on RT RNase H Ile methyl resonances. (**a**) Overlay of the $^{1}H–^{13}C$ HMQC spectra of the 15 μM [$^{13}C\delta H_3$-Ile]RNase H domain (black), 20 μM RNase H plus 20 μM $Zn^{2+}$ (red). (**b**) Overlayed spectra of 20 μM [$^{13}C\delta H_3$-Ile]Rnase H with 20 μM $Zn^{2+}$ (red) and with 40 μM $Zn^{2+}$ (blue). **c**) Overlayed spectra of 15 μM [$^{13}C\delta H_3$-Ile]RNase H (black), 20 μM [$^{13}C\delta H_3$-Ile]RNase H with 40 μM $Zn^{2+}$(blue) and 20 μM [$^{13}C\delta H_3$-Ile]Rnase H with 16 mM $Zn^{2+}$-ATP (magenta).

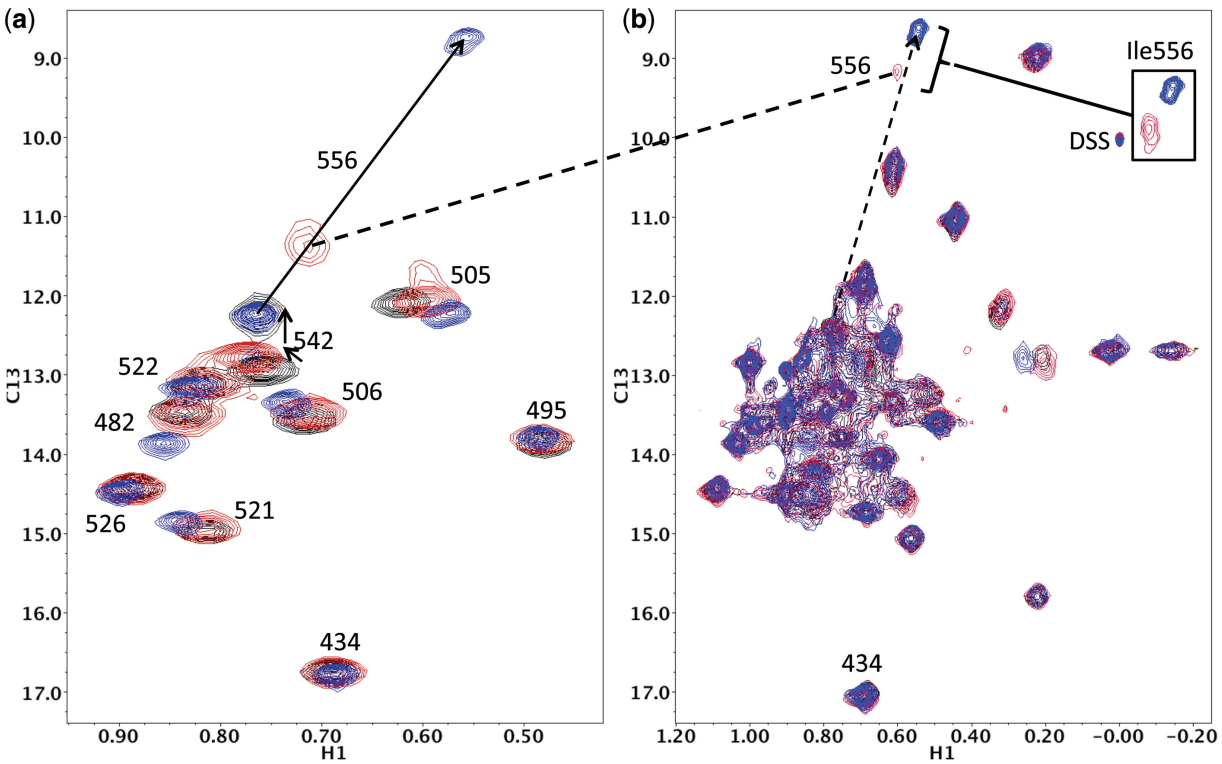


**Figure 4.** Effect of $Mg^{2+}$ and 2-Hydroxyisoquinoline-1,3(2H,4H)-dione ligands on RNase H Ile resonances. (**a**) Overlay of the $^{1}H–^{13}C$ HMQC spectra of the isolated [$^{13}C\delta H_3$-Ile]RNase H domain (black), plus 4 mM $Mg^{2+}$ (red), after subsequent addition of 0.5 mM isoquinolone (blue). (**b**) Overlayed $^{1}H–^{13}C$ HMQC spectra of 50 μM apo [$^{13}C\delta H_3$-Ile]$_{66}$RT (black), +4 mM $Mg^{2+}$ (red), after a subsequent addition of 0.5 mM 2-Hydroxyisoquinoline-1,3(2H,4H)-dione (blue). The inset in Figure 3b shows the Ile556 resonances plotted with a lower threshold. In addition to the dramatic shift of Ile556, a few other isoleucine resonances experience small shift perturbations.

interacts with the p51 subunit. The interface includes a hydrophobic-binding pocket on p51 that interacts with Ile542 and, in some structures, additional hydrogen bonding interactions between Arg284$_{51}$ and residues Gln547 and/or Glu546 on the RNase H domain (Figure 6). We thus conclude that the interaction of the RNase H domain on the p66 subunit with the thumb subdomain on the p51 subunit, helps to orient helix E,

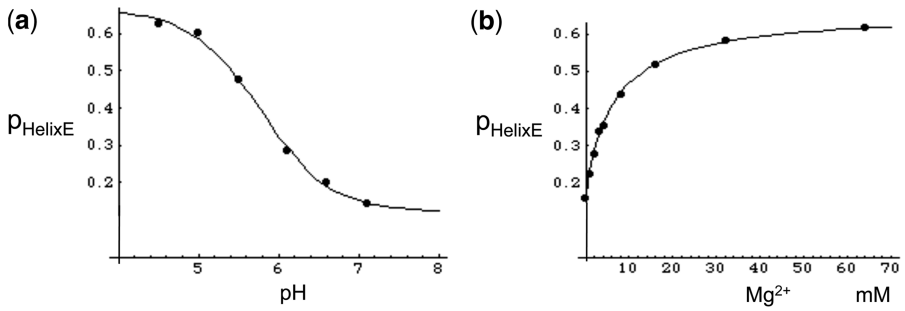


**Figure 5.** Dependence of helix E probability on pH and $Mg^{2+}$. The helix probability factor, calculated from the Ile556 δ1-methyl $^{13}C$ shift using Equation (4) and fit to the relations described in 'Materials and Methods' section, is shown as a function of pH (**a**) and [$Mg^{2+}$] (**b**).

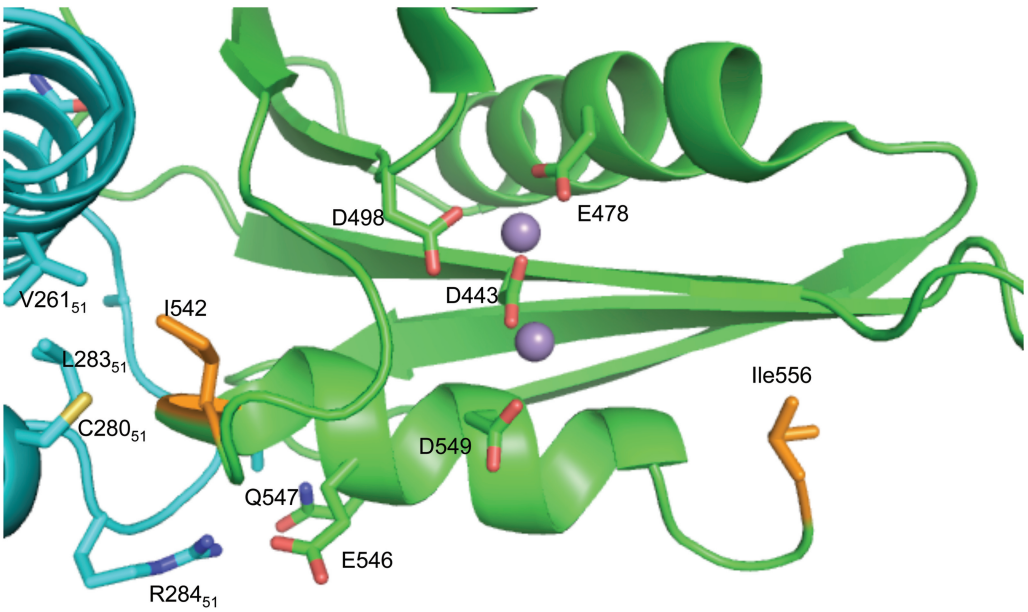


**Figure 6.** Intersubunit interactions contribute to RNase H domain helix E stability. The N-terminus of the RNase H domain helix E (green) is stabilized by hydrophobic interactions involving Ile542 and residues of the p51 subunit (cyan) and by hydrogen bonding interactions involving Arg244 on p51, and E546 and Q547 on the RNase H domain (pdb code: 3QIP). The RNase H inhibitor is omitted from the figure to allow clearer visualization of the interactions.

leading to a more completely preformed $Mg_A$-binding site with higher $Mg^{2+}$ affinity, so that addition of a fixed concentration of $Mg^{2+}$ leads to a greater shift of 9.2 ppm for Ile556. Based on the observed Ile556 $^{13}C$ shift of 9.2 ppm, we obtain $p_{HelixE} = 86\%$ for the RH domain of RT, compared with 35% for the isolated RNase H domain, both evaluated in the presence of 4 mM $MgCl_2$. Addition of the isoquinolone inhibitor leads to a more extreme shift of the Ile556 methyl resonance and eliminates the exchange broadening, consistent with a well-defined helix orientation. In contrast with the result obtained in the presence of $Mg^{2+}$, the Ile556 resonance shifts observed for the ternary complexes of both RT and the isolated RNase H domain with $Mg^{2+}$-isoquinolone are similar. In general, the relative rarity of the $\chi 2 = g-$ shift conformation makes it easy to identify the corresponding resonances even in enzymes such as RT that contain many isoleucine residues.

An analogous difference of pH sensitivity was also observed between the isolated RH domain and intact RT. At pH 6.1, Ile556 $\delta^{13}C = 11.7$ ppm for the isolated RH domain, and 9.6 ppm in RT (data not shown). It thus appears likely that the additional structural features present in RT that help to preform the $Mg_A$-binding site also lead to elevation of the p*K* value that characterizes the Ile556 shift. This result is consistent with the presence of a bridging interaction in which Asp443 and Asp549 share a proton.

## Structural and catalytic role of Arg557

The data presented above support the conclusion that the conformations of the C-terminal residues observed in the recently determined inhibitor-complex structures, which are not apparent in structures of the apo enzyme, can be significantly populated at low pH or in the presence of divalent ions. In addition to the role of Ile556 in stabilizing the orientation of helix E, this structural analysis also supports a functional role for Arg557, in orienting the active site Asp549 residue, stabilizing the

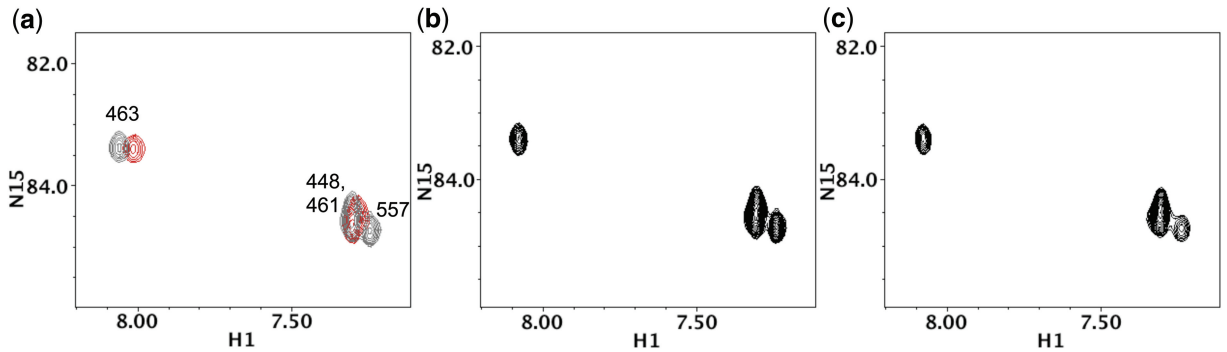


**Figure 7.** Arginine NHε spectra of RT RNase H domain. A region of the $^{1}H$–$^{15}N$ HSQC spectra of U-[$^{15}N$]RNase H containing the Arginine NHε resonances. (**a**) apo RNase H (black) overlayed with RNase H (R557S) (red); (**b**) RNase H + 200 μM $Zn^{2+}$, (**c**) RNase H + 200 μM $Zn^{2+}$ + 100 μM ATP. The I(463):I(448+461):I(557) intensity ratio in panel b is 1:2.1:1.4, and in panel c 1:2.1:0.7. All NMR samples contained 50 μM RNase H in 25 mM Tris–d11, pH 5.5, containing 8% $D_2O$ for the lock, 25°C.

helix E structure, and presumably interacting with the RNA strand of the substrate.

In order to better characterize the behavior of Arg557, we obtained $^{1}H$–$^{15}N$ HSQC spectra of the region containing the arginine NHε resonances at pH 5.5, at which the slower exchange of Hε facilitates the observations (Figure 7). The well-resolved resonance is assigned to Arg463 on the basis of structures showing a side-bonded guanidino group of this residue with the carboxylate of Glu438 [e.g. pdb 3K2P, (34)]. This salt bridge plays an important role in limiting the accessibility of the Phe440–Tyr441 protease cleavage site in the RNase H domain (43). Two other Arg NHε resonances are observed, with an intensity ratio of 2:1. The Arg557 resonance was assigned based on the spectrum of an RNase H(R557S) mutant as indicated in Figure 7, and the remaining resonance, with approximately double the intensity of each resolved peak, corresponds to Arg448 and Arg461. The resolution of the Arg557 NHε resonance, despite the fact that Hε is not involved in a hydrogen bond, is consistent with the positional constraint of the Arg557 guanidino group. In contrast, the NHε resonances for Arg448 and Arg461 are degenerate. A small upfield shift for the Hε resonance of Arg463 is also observed for the RNase H (R557S) mutant. Presumably, this results from a longer range influence of the helix E structure on the adjacent β-sheet, which includes Arg463.

The limiting shift of Ile556 observed in the presence of both $Mg^{2+}$ and the isoquinolone inhibitor is also somewhat smaller for the R557S mutant ($\delta^{13}C$ = 9.8 ppm; Supplementary Figures S7). We interpret this difference as a consequence of the backbone restraint imposed by positioning of the Arg557 sidechain. In the absence of this conformational restraint, the backbone of the adjacent Ile556 is also less constrained and this will also influence the sidechain conformation as it packs against the β-sheet and the Lys454 sidechain.

### Identification of a new RNase H ternary complex

Coupling of the $^{13}C$ shift of Ile556 Cδ with the position of helix E and assembly of the active site makes this resonance well suited as a sensitive probe for the discovery of new RNase H active site complexes. The location of the probe >10 Å from the active site itself suggests that the shift should be sensitive to how well positioned the helix is, without being strongly dependent on the detailed nature of the ligand complex. After surveying a series of divalent cations and available ligands, we found that $Zn^{2+}$-ATP was also capable of producing a shift of the Ile556 Cδ resonance that was similar to that produced by the $Mg^{2+}$–isoquinolone inhibitor complex (Figures 3c and 4b).

We also investigated the effect of this ternary complex on the behavior of the $^{1}H$–$^{15}N$ HSQC spectrum containing the arginine NHε resonances. Addition of 200 μM $Zn^{2+}$ to the sample at pH 5.5 resulted in small decreases in intensity of several resonances. In contrast, addition of 200 μM $Zn^{2+}$ + 100 μM ATP decreased the intensity of the Arg557 resonance by ~50% (Figure 7c). The most probable interpretation of this result is that the bound Zn-ATP helps to restrain the position of the Arg557 sidechain, resulting in a decreased $T_2$ value, reduced polarization transfer and hence reduced resonance intensity, although several alternative interpretations are also possible. Regardless of the basis for the intensity perturbation, this observation is consistent with the suggestion above that the Arg557 guanidinium sidechain helps to stabilize the interaction of the negatively charged Asp549 sidechain and a negatively charged ligand—either the substrate or in this case, ATP.

## DISCUSSION

Concepts regarding the structure and catalytic mechanism of RNase H enzymes have undergone a considerable transformation in recent years as a result of the availability of crystal structure data for several RNase H–RNA•DNA complexes (2,3). These structures demonstrate the critical contribution of the substrate to the divalent ion-binding sites. In contrast with these results, the structure of an RNase H complex with dsDNA lacks both of the bound divalent ions (44). In combination with the characterization of the dynamic state of the apo RT RNase H domain, these structures demonstrate the major role that the hybrid RNA•DNA substrate plays not just for divalent ion binding, but for the creation of the active

site. Although the active sites of most enzymes are highly pre-organized to make optimal and highly discriminating contacts with the substrate, the results presented above for the RT RNase H domain demonstrate that the active site is quite dynamic and lacks significant structural integrity in the absence of the substrate. Even $Mg^{2+}$ concentrations well in excess of normal physiological levels of ~1 mM (45,46) only are able to partially overcome the lack of pre-organization, while the addition of a specifically designed inhibitor results in a more significant stabilization of the active site structure. Under physiologic conditions, this low $Mg^{2+}$ affinity is alternatively overcome as a result of synergistic binding of $Mg^{2+}$ with the hybrid RNA•DNA substrate. These studies thus support the conclusion that substrate-induced active site stabilization plays a major role in the determination of enzymatic substrate specificity. Recognition and activation are thus not achieved by a preformed active site, but by requiring the substrate nucleotide to complete the formation of the active site of the enzyme.

Although there is little data on the solution behavior of the *Bacillus halodurans* RNase H, the more significant lack of stabilizing elements in the structure suggests that it too relies on substrate binding for formation of the active site complex. Nowotny and Yang (4) propose that product release is likely to require dissociation of $Mg_A$, so that the poor active site stability may contribute to product release. Since the Tyr441 sidechain interacts directly with Gly544 in helix E, partial disorder of helix E in the absence of ligands may also facilitate the unfolding of one RNase H domain, which is required to allow HIV protease access to the F440–Y441 cleavage site (39).

These studies also suggest a functional role for Arg557 in the catalytic activity of RT RNase H. A structure of the complex of RT RNase H domain with an RNA•DNA hybrid (Figure 2b) was generated by superposition with the structure of the human RNase HI in complex with an RNA•DNA (pdb code: 2QKK) (3). The sidechain of Lys454 interrupts the progress of helix E, forcing the backbone to loop around so that Arg557 is positioned to form a salt bridge with Asp549. This leads to a positional similarity of the guanidine sidechain of Arg278 in the human enzyme with Arg557 in RT RNase H, suggesting a functional equivalence that is not apparent from the sequence alignment (3). It is likely that this residue facilitates substrate binding by reducing the electrostatic repulsion between Asp549 and the negatively charged phosphate groups on the substrate. The effect of the $Zn^{2+}$-ATP ligand on the Arg557 NHε resonance intensity (Figure 7c) supports the significance of an analogous interaction between Arg557 guanidinium group and the negatively charged substrate.

As demonstrated here, $Mg^{2+}$ possesses a limited ability to stabilize the active site; its limiting effect on helix stability is in fact similar to the effect of low pH; both $Mg^{2+}$ and $H^+$ produce asymptotic limits of the helix E formation probability of ~2/3. Based on the concentration dependence of helix E stabilization, at least some of the effect of the $Mg^{2+}$ appears to result from partial occupancy of the two divalent ion-binding sites. $Mn^{2+}$ has been widely used as a $Mg^{2+}$ substitute in X-ray crystallographic studies due to its chemical similarity and its anomalous scattering at the copper Kα wavelength. The tighter binding of $Mn^{2+}$ to both the *E. coli* and RT RNase H enzymes is reflected in the ability to form two-ion complexes, while no complexes containing both catalytic $Mg^{2+}$ ions have been observed in the absence of substrate or inhibitor. As shown in this study, $Zn^{2+}$ provides an attractive diamagnetic alternative to $Mn^{2+}$ for some NMR studies, with the tighter binding leading to more complete helix stabilization and allowing a clean discrimination of the two divalent ion-binding sites. Typical $Mg^{2+}$ dissociation constants often exceed the conveniently accessible protein concentrations used for NMR studies, making it difficult to identify specific binding interactions. Alternatively, the $Zn^{2+}$ dissociation constants will often be lower than the enzyme concentrations used for NMR studies, allowing better identification of specific binding interactions. Consistent with these observations, $Zn^{2+}$ is able to support RT RNase H activity at ~25 μM, significantly below the millimolar concentrations of $Mg^{2+}$ that are typically required (41).

The differential effects of the metal ions on helix E stability provide additional insight into one of the more puzzling observations related to RNase H domain activity. As summarized above, the isolated RT RNase H domain has negligible activity (47–49). However, modifications that enhance substrate-binding affinity such as the addition of His-tags or the inclusion of substrate-binding residues derived from the *E. coli* enzyme are able to restore $Mn^{2+}$ activity, but not $Mg^{2+}$-dependent activity. The significantly greater abilities of $Zn^{2+}$ and $Mn^{2+}$ compared with $Mg^{2+}$ to bind to both divalent ion sites in the absence of substrate suggests a weaker requirement for substrate-induced positioning of the ions. Thus, consistent with the substrate-dependent specificity behavior outlined above, correctly positioned $Mn^{2+}$ ions may be able to compensate for poorer substrate positioning, while the proper orientation of the $Mg^{2+}$ ions is fully dependently on correct substrate positioning. The inability of bound dsDNA to support divalent metal ion binding to the *B. halodurans* RNase H (44), is also consistent with this general view that correct substrate positioning is critical to the correct binding of $Mg^{2+}$.

### Ile556 shift as a basis for ligand screening

Another significant implication of the present study is the utility of conformationally-induced shifts such as are observed for Ile556, as a basis for ligand screening. Isotopically labeled ILV methyl groups provide a useful basis for identifying ligand-binding sites by chemical shift mapping (50). Interestingly, the total $^{13}C$ shift of −3.6 ppm observed for the Ile556 methyl resonance is larger than any of the reported direct methyl shift contributions observed in a study designed to map ligand-binding sites (50). In general, it is probably straightforward to distinguish these effects since, as in the present case, the conformationally mediated *g*/*t* transitions occur for residues that are remote from the binding site and typically buried in the protein interior, while surface residues are more likely to adopt the lower energy *trans* conformation and to experience direct ligand-induced

shifts. For the RNase H domain, either isolated or as part of RT, the Ile 556 resonance provides a direct readout of the stabilization of helix E that is expected to be essentially independent of the details of ligand binding. The feasibility of using the Ile556 shift in this way is illustrated by our discovery of an RNase H•$Zn^{2+}$•ATP complex, the details of which are currently under investigation.

## SUPPLEMENTARY DATA

Supplementary Data are available at NAR Online: Supplementary Figures 1–7.

## ACKNOWLEDGEMENTS

The authors thank Dr Joseph Krahn, Dr. Matt Cuneo, Dr. Tom Kirby and Dr. Jason Williams for thoughtful comments on the manuscript.

## FUNDING

Research Project Number Z01-ES050147 to R.E.L. in the Intramural Research Program of the National Institute of Environmental Health Sciences, National Institutes of Health. E.F.D. is supported by National Institutes of Health, NIEHS, under Delivery Order HHSN273200700046U. Chemical synthesis of 2-hydroxyisoquinoline-1,3(2H,4H)-dione was performed for the National Institute of Environmental Health Sciences, National Institutes of Health, U.S. Department of Health and Human Services, under contract No. HHSN273201100001C. Funding for open access charge: Research Project Number Z01-ES050147 to R.E.L. in the Intramural Research Program of the National Institute of Environmental Health Sciences, National Institutes of Health.

*Conflict of interest statement*. None declared.

## REFERENCES

1. Beilhartz,G.L. and Gotte,M. (2010) HIV-1 ribonuclease H: structure, catalytic mechanism and inhibitors. *Viruses Basel*, **2**, 900–926.
2. Nowotny,M., Gaidamakov,S.A., Crouch,R.J. and Yang,W. (2005) Crystal structures of RNase H bound to an RNA/DNA hybrid: substrate specificity and metal-dependent catalysis. *Cell*, **121**, 1005–1016.
3. Nowotny,M., Gaidamakov,S.A., Ghirlando,R., Cerritelli,S.M., Crouch,R.J. and Yang,W. (2007) Structure of human RNase h1 complexed with an RNA/DNA hybrid: insight into HIV reverse transcription. *Mol. Cell*, **28**, 264–276.
4. Nowotny,M. and Yang,W. (2006) Stepwise analyses of metal ions in RNase H catalysis from substrate destabilization to product release. *EMBO J.*, **25**, 1924–1933.
5. Ho,M.H., De Vivo,M., Dal Peraro,M. and Klein,M.L. (2010) Understanding the effect of magnesium ion concentration on the catalytic activity of ribonuclease H through computation: does a third metal binding site modulate endonuclease catalysis? *J. Am. Chem. Soc.*, **132**, 13702–13712.
6. Rosta,E., Nowotny,M., Yang,W. and Hummer,G. (2011) Catalytic mechanism of RNA backbone cleavage by ribonuclease H from quantum mechanics/molecular mechanics simulations. *J. Am. Chem. Soc.*, **133**, 8934–8941.
7. Rausch,J.W. and LeGrice,S.F.J. (1997) Reverse transcriptase-associated ribonuclease H activity as a target for antiviral chemotherapy. *Antivir. Chem. Chemoth.*, **8**, 173–185.
8. Klumpp,K. and Mirzadegan,T. (2006) Recent progress in the design of small molecule inhibitors of HIV RNase H. *Curr. Pharm. Design*, **12**, 1909–1922.
9. Tramontano,E. and Di Santo,R. (2010) HIV-1 RT-associated RNase H function inhibitors: recent advances in drug development. *Curr. Med. Chem.*, **17**, 2837–2853.
10. Yu,F., Liu,X.Y., Zhan,P. and De Clercq,E. (2008) Recent advances in the research of HIV-1 RNase H inhibitors. *Mini Rev. Med. Chem.*, **8**, 1243–1251.
11. Ghosh,M., Howard,K.J., Cameron,C.E., Benkovic,S.J., Hughes,S.H. and Legrice,S.F.J. (1995) Truncating alpha-helix E' of P66 human-immunodeficiency-virus reverse-transcriptase modulates rnase-h function and impairs DNA strand transfer. *J. Biol. Chem.*, **270**, 7068–7076.
12. Rausch,J.W., Sathyanarayana,B.K., Bona,M.K. and Le Grice,S.F.J. (2000) Probing contacts between the ribonuclease H domain of HIV-1 reverse transcriptase and nucleic acid by site-specific photocross-linking. *J. Biol. Chem.*, **275**, 16015–16022.
13. Roquebert,B. and Marcelin,A.G. (2008) The involvement of HIV-1 RNAse H in resistance to nucleoside analogues. *J. Antimicrob. Chemoth.*, **61**, 973–975.
14. Goedken,E.R., Raschke,T.M. and Marqusee,S. (1997) Importance of the C-terminal helix to the stability and enzymatic activity of Escherichia coli ribonuclease H. *Biochemistry*, **36**, 7256–7263.
15. Kern,G., Handel,T. and Marqusee,S. (1998) Characterization of a folding intermediate from HIV-1 ribonuclease H. *Protein Sci.*, **7**, 2164–2174.
16. Powers,R., Clore,G.M., Bax,A., Garrett,D.S., Stahl,S.J., Wingfield,P.T. and Gronenborn,A.M. (1991) Secondary structure of the ribonuclease-H domain of the human-immunodeficiency-virus reverse-transcriptase in solution using 3-dimensional double and triple resonance heteronuclear magnetic-resonance spectroscopy. *J. Mol. Biol.*, **221**, 1081–1090.
17. Powers,R., Clore,G.M., Stahl,S.J., Wingfield,P.T. and Gronenborn,A. (1992) Analysis of the backbone dynamics of the ribonuclease-H domain of the human-immunodeficiency-virus reverse-transcriptase using N-15-relaxation measurements. *Biochemistry*, **31**, 9150–9157.
18. Pari,K., Mueller,G.A., DeRose,E.F., Kirby,T.W. and London,R.E. (2003) Solution structure of the RNase H domain of the HIV-1 reverse transcriptase in the presence of magnesium. *Biochemistry*, **42**, 639–650.
19. London,R.E., Wingad,B.D. and Mueller,G.A. (2008) Dependence of amino acid side chain C-13 shifts on dihedral angle: application to conformational analysis. *J. Am. Chem. Soc.*, **130**, 11097–11105.
20. Mulder,F.A.A. (2009) Leucine Sidechain Conformation and dynamics in proteins from C-13 NMR chemical shifts. *Chembiochem*, **10**, 1477–1479.
21. Hansen,D.F., Neudecker,P. and Kay,L.E. (2010) Determination of Isoleucine Sidechain Conformations in Ground and Excited States of Proteins from Chemical Shifts. *J. Am. Chem. Soc.*, **132**, 7589–7591.
22. Butterfoss,G.L., DeRose,E.F., Gabel,S.A., Perera,L., Krahn,J.M., Mueller,G.A., Zheng,X.H. and London,R.E. (2010) Conformational dependence of (13)C shielding and coupling constants for methionine methyl groups. *J. Biomol. NMR*, **48**, 31–47.
23. Zheng,X.H., Mueller,G.A., DeRose,E.F. and London,R.E. (2009) Solution characterization of [methyl-(13)C]methionine HIV-1 reverse transcriptase by NMR spectroscopy. *Antivir. Res.*, **84**, 205–214.
24. Tugarinov,V., Hwang,P.M., Ollerenshaw,J.E. and Kay,L.E. (2003) Cross-correlated relaxation enhanced H-1-C-13 NMR spectroscopy of methyl groups in very high molecular weight proteins and protein complexes. *J. Am. Chem. Soc.*, **125**, 10420–10428.
25. Mueller,G.A., Pari,K., DeRose,E.F., Kirby,T.W. and London,R.E. (2004) Backbone dynamics of the RNase H domain of HIV-1 reverse transcriptase. *Biochemistry*, **43**, 9332–9342.

26. Leitner,T., McCutchan,F., Foley,B., Mellors,J., Hahn,B., Wolinsky,S., Marx,P. and Korber,B. (2005) *HIV Sequence Compendium 2005*, Theoretical Biology and Biophysics Group, Los Alamos National Laboratory, NM, LA-UR 04-7420.
27. Sprangers,R. and Kay,L.E. (2007) Quantitative dynamics and binding studies of the 20S proteasome by NMR. *Nature*, **445**, 618–622.
28. Gelis,I., Bonvin,A.M.J.J., Keramisanou,D., Koukaki,M., Gouridis,G., Karamanou,S., Economou,A. and Kalodimos,C.G. (2007) Structural basis for signal-sequence recognition by the translocase motor SecA as determined by NMR. *Cell*, **131**, 756–769.
29. Billamboz,M., Bailly,F., Barreca,M.L., De Luca,L., Mouscadet,J.F., Calmels,C., Andreola,M.L., Witvrouw,M., Christ,F., Debyser,Z. *et al.* (2008) Design, synthesis, and biological evaluation of a series of 2-hydroxyisoquinoline-1,3(2H,4H)-diones as dual inhibitors of human immunodeficiency virus type 1 integrase and the reverse transcriptase RNase H domain. *J. Med. Chem.*, **51**, 7717–7730.
30. Delaglio,F., Grzesiek,S., Vuister,G.W., Zhu,G., Pfeifer,J. and Bax,A. (1995) NMRPipe: a multidimensional spectral processing system based on UNIX pipes. [see comments]. *J. Biomol. NMR*, **6**, 277–293.
31. Johnson,B.A. and Blevins,R.A. (1994) NMRVIEW: a computer program for the visualization and analysis of NMR data. *J. Biomol. NMR*, **4**, 603–614.
32. Cheney,B.V. and Grant,D.M. (1967) Carbon-13 magnetic resonance.8. Theory of carbon-13 chemical shifts applied to saturated hydrocarbons. *J. Am. Chem. Soc.*, **89**, 5319–5327.
33. Grant,D.M. and Cheney,B.V. (1967) Carbon-13 magnetic resonance.7. Steric perturbation of carbon-13 chemical shift. *J. Am. Chem. Soc.*, **89**, 5315–5318.
34. Himmel,D.M., Maegley,K.A., Pauly,T.A., Bauman,J.D., Das,K., Dharia,C., Clark,A.D., Ryan,K., Hickey,M.J., Love,R.A. *et al.* (2009) Structure of HIV-1 reverse transcriptase with the inhibitor beta-thujaplicinol bound at the rNase H active site. *Structure*, **17**, 1625–1635.
35. Kirschberg,T.A., Balakrishnan,M., Squires,N.H., Barnes,T., Brendza,K.M., Chen,X.W., Eisenberg,E.J., Jin,W.L., Kutty,N., Leavitt,S. *et al.* (2009) RNase H active site inhibitors of human immunodeficiency virus Type 1 reverse transcriptase: design, biochemical activity, and structural information. *J Med Chem*, **52**, 5781–5784.
36. Lansdon,E.B., Liu,Q., Leavitt,S.A., Balakrishnan,M., Perry,J.K., Lancaster-Moyer,C., Kutty,N., Liu,X.H., Squires,N.H., Watkins,W.J. *et al.* (2011) Structural and binding analysis of pyrimidinol carboxylic acid and N-hydroxy quinazolinedione HIV-1 RNase H inhibitors. *Antimicrob. Agents Ch.*, **55**, 2905–2915.
37. Su,H.P., Yan,Y.W., Prasad,G.S., Smith,R.F., Daniels,C.L., Abeywickrema,P.D., Reid,J.C., Loughran,H.M., Kornienko,M., Sharma,S. *et al.* (2010) Structural basis for the inhibition of RNase H activity of HIV-1 reverse transcriptase by RNase H active site-directed inhibitors. *J. Virol.*, **84**, 7625–7633.
38. Oda,Y., Yamazaki,T., Nagayama,K., Kanaya,S., Kuroda,Y. and Nakamura,H. (1994) Individual ionization-constants of all the carboxyl groups in Ribonuclease Hi from Escherichia-Coli determined by Nmr. *Biochemistry*, **33**, 5275–5284.
39. Davies,J.F., Hostomska,Z., Hostomsky,Z., Jordan,S.R. and Matthews,D.A. (1991) Crystal-structure of the ribonuclease-H domain of Hiv-1 reverse-transcriptase. *Science*, **252**, 88–95.
40. Goedken,E.R. and Marqusee,S. (2001) Co-crystal of Escherichia coli RNase HI with Mn2+ ions reveals two divalent metals bound in the active site. *J. Biol. Chem.*, **276**, 7266–7271.
41. Fenstermacher,K.J. and DeStefano,J.J. (2011) Mechanism of HIV reverse transcriptase inhibition by zinc. Formation of a highly stable enzyme-(primer-template) complex with profoundly diminished catalytic activity. *J. Biol. Chem.*, **286**, 40433–40442.
42. Wishart,D.S., Bigam,C.G., Holm,A., Hodges,R.S. and Sykes,B.D. (1995) H-1, C-13 and N-15 Random coil Nmr chemical-shifts of the common amino-acids.1. Investigations of nearest-neighbor effects (Vol 5, Pg 67, 1995). J. Biomol. NMR, 5, 332–332.
43. Navarro,J.M., Damier,L., Boretto,J., Priet,S., Canard,B., Querat,G. and Sire,J. (2001) Glutamic residue 438 within the protease-sensitive subdomain of HIV-1 reverse transcriptase is critical for heterodimer processing in viral particles. *Virology*, **290**, 300–308.
44. Pallan,P.S. and Egli,M. (2008) Insights into RNA/DNA hybrid recognition and processing by RNase H from the crystal structure of a non-specific enzyme-dsDNA complex. *Cell Cycle*, **7**, 2562–2569.
45. Corkey,B.E., Duszynski,J., Rich,T.L., Matschinsky,B. and Williamson,J.R. (1986) Regulation of free and bound magnesium in rat hepatocytes and isolated-mitochondria. *J. Biol. Chem.*, **261**, 2567–2574.
46. Murphy,E., Steenbergen,C., Levy,L.A., Raju,B. and London,R.E. (1989) Cytosolic free magnesium levels in ischemic rat-heart. *J. Biol. Chem.*, **264**, 5622–5627.
47. Evans,D.B., Brawn,K., Deibel,M.R., Tarpley,W.G. and Sharma,S.K. (1991) A recombinant ribonuclease-H domain of Hiv-1 reverse-transcriptase that is enzymatically active. *J. Biol. Chem.*, **266**, 20583–20585.
48. Becerra,S.P., Clore,G.M., Gronenborn,A.M., Karlstrom,A.R., Stahl,S.J., Wilson,S.H. and Wingfield,P.T. (1990) Purification and characterization of the Rnase H domain of Hiv-1 reverse-transcriptase expressed in recombinant Escherichia-Coli. *FEBS lett.*, **270**, 76–80.
49. Stahl,S.J., Kaufman,J.D., Vikictopic,S., Crouch,R.J. and Wingfield,P.T. (1994) Construction of an enzymatically active ribonuclease-H domain of human-immunodeficiency-virus type-1 reverse-transcriptase. *Protein Engineer.*, **7**, 1103–1108.
50. Hajduk,P.J., Augeri,D.J., Mack,J., Mendoza,R., Yang,J.G., Betz,S.F. and Fesik,S.W. (2000) NMR-based screening of proteins containing (13)C-labeled methyl groups. *J. Am. Chem. Soc.*, **122**, 7898–7904.